



Schwarzschild Black Hole in Galaxies Surrounded by a Dark Matter Halo

Ahmad Al-Badawi 

Department of Physics, Al-Hussein Bin Talal University, P. O. Box: 20, 71111, Ma'an,
Jordan. E-mail: ahmadbadawi@ahu.edu.jo

Sanjar Shaymatov 

Institute for Theoretical Physics and Cosmology, Zhejiang University of Technology,
Hangzhou 310023, China

Institute of Fundamental and Applied Research, National Research University TIIAME,
Kori Niyoziy 39, Tashkent 100000, Uzbekistan

University of Tashkent for Applied Sciences, Str. Gavhar 1, Tashkent 100149, Uzbekistan
Western Caspian University, Baku AZ1001, Azerbaijan

E-mail: sanjar@astrin.uz

Yassine Sekhmani 

Center for Theoretical Physics, Khazar University, 41 Mehseti Street, Baku, AZ1096,
Azerbaijan.

Centre for Research Impact and Outcome, Chitkara University Institute of Engineering
and Technology, Chitkara University, Rajpura, 140401, Punjab, India

Chitkara Centre for Research and Development, Chitkara University, Baddi, Himachal
Pradesh, 174103, India

E-mail: sekhmaniyassine@gmail.com

Abstract

In this paper, we derive a novel Schwarzschild-like black hole (BH) solution describing a static and asymptotically flat BH surrounded by a dark matter (DM) halo with a Dehnen-type density distribution in the surrounding environment. We investigate the properties of the obtained BH by studying the curvature properties and energy conditions in Einstein gravity. Furthermore, we explore the features of a novel Schwarzschild-like BH embedded in a DM halo with Dehnen-type density profile by analyzing the timelike geodesics of particles along with BH observable properties.

I. INTRODUCTION

Our universe contains massive objects such as BHs that play crucial roles in Einstein's general relativity and other gravity theories, making the idea that they are completely isolated in our universe implausible. BHs probably live in dynamic and complex surroundings. In example, there is considerable evidence that supermassive BHs are the driving forces underlying active galactic nuclei [1, 2]. There is also strong evidence that DM surrounds most galaxies in a halo [3]. Furthermore, astronomical evidence for DM can be found in measurements of galactic rotation curves [4], bullet clusters [5], baryon acoustic oscillations and cosmic microwave background [6] and large-scale structure development of the universe [7]. These observations are unlikely to have satisfactory interpretations unless we assume a large amount of DM in our universe. The cosmic microwave background observation shows that the Universe is composed mostly of DM (27%) and dark energy (68%). Several unknown particles predicted by theories beyond the Standard Model are potential candidates for DM [8–11], including weakly interacting massive particles (WIMPs), axions, and sterile neutrinos. A halo of DM surrounds most galaxies as well [3], which could have significant effects on supermassive BHs. The investigation of DM halo effects on supermassive BHs is therefore of great importance, as it allows us to gain a better understanding of how DM interacts with BHs. There are many effects of DM halo structures on galactic rotation curves [3–5, 12], matter motion observed in bullet cluster collisions [13], BH shadows and polarized images [14, 15] and gravitational lensing of massive objects [16, 17].

It is worth noting that, despite the fact that DM is only known for its gravitational interaction feature, there is strong evidence confirming the presence of DM in the universe (see, for example, [18–20]). It is a well-established fact through observations that stars can be formed in particular regions of galaxies, i.e., very close to their centers. This results in a galactic DM halo being formed in the surrounding regions of host galaxies. Hence, host galaxies (i.e., spiral or giant elliptical galaxies) are formed in the presence of a DM halo (see, for example, [21–24]). Analyzing DM models can help enhance our understanding of its fundamental nature, despite being a long-standing problem GR. Based on observational data, the DM halo only helps explain the rotational velocity of stars orbiting host galaxies [25]. Many different DM halo models have been developed based on simulation studies and astrophysical data. Various BH solutions have since been developed, such as those involving

a DM profile associated with a phantom scalar field [26], explored with extensive analyses providing some insights into the nature of DM profile [27–32] and analytical models that exhibit a supermassive BH solution immersed in a DM halo (see, e.g., [33–35]). Besides, the Navarro-Frenk-White model [36], the Einasto model [37, 38], the Burkert model [39], and Dehnen model [40]. Recently, a lot of studies into the Dehnen-type DM halo effects on BHs have been conducted from various perspectives. In Ref. [41], the authors investigate the impact of density profile slopes on the survivability of low star-formation efficiency star clusters following immediate gas expulsion. To accomplish this goal, they examine scenarios in which a star cluster has a Plummer profile and a Dehnen profile with cusps of differing slopes at the time of formation. Other BH solution with the Dehnen DM halo profile is constructed in [42] for the study of an ultrafaint dwarf galaxy. Further, in [43] a new BH solution is surrounded by a Dehnen-(1,4,0) type DM halo created by embedding a Schwarzschild black hole within the halo, resulting in a composite DM-BH system. This study [43] examines the thermodynamics of the effective BH spacetime and its null geodesic.

In this paper, we present a new Schwarzschild-like BH solution describing a static and asymptotically flat BH surrounded by a DM halo with a Dehnen-type density profile $(1, 4, 5/2)$ in its surroundings. To achieve this aim, we employ the method developed in Ref. [44], which has also been used by the authors of Ref. [45]. We examine the singularity structure of this BH at $r = 0$, focusing on analyzing the spacetime curvature invariants and then consider the energy conditions in Einstein gravity. Finally, we delve into how the DM profile affects particles’ timelike geodesics, enhancing our understanding of the effects of the DM halo profile on particle geodesics.

The paper is organized in a following way: In Sec. II, we obtain the metric function of the BH-DM profile by examining the theoretical framework of the Dehnen-type density distribution. Sec. III examines the singularity structure and then the energy conditions in Einstein gravity. In Sec. IV, we investigate the timelike geodesics of massive particles with the rest mass around the Schwarzschild-like BH immersed in the DM halo within a Dehnen-type density profile. Finally, we end up with our remarks and conclusions in Sec. V.

II. SCHWARZSCHILD-LIKE BH METRIC IMMERSSED IN THE DM HALO

In this section, we utilize the method developed in Ref. [44] and later employed by Ref. [45] to determine the Schwarzschild-like BH metric in the DM halo within a Dehnen-type density distribution. This method typically consists of two steps: First, in the case of general relativity, the DM spacetime metric is constructed using the DM profile; second, the approximate solution for the BH under DM is derived by analyzing Einstein's field equations. The first step towards a Schwarzschild BH is to understand the mass distribution of a Dehnen-type DM halo. In a spherically symmetric spacetime, the mass distribution is determined by the DM density profile. The mass profile is given by [46]:

$$M_D = 4\pi \int_0^r \rho(r') r'^2 dr', \quad (1)$$

where the density profile of the Dehnen type DM halo is given by

$$\rho = \rho_s \left(\frac{r}{r_s}\right)^{-\gamma} \left[\left(\frac{r}{r_s}\right)^\alpha + 1 \right]^{\frac{\gamma-\beta}{\alpha}}, \quad (2)$$

where, ρ_s and r_s are the central halo density radius. Whereas γ determines the specific variant of the profile. The values of γ lies within $[0, 3]$ i.e. $\gamma = 3/2$ is used to fit the surface brightness profiles of elliptical galaxies which closely resembles the de Vaucouleurs $r^{1/4}$ profile [47]. In this work, we use the Dehnen- $(\alpha, \beta, \gamma) = (1, 4, 5/2)$ DM halo. Hence Eq. (2) becomes

$$\rho = \frac{\rho_s}{\left(\frac{r}{r_s}\right)^{5/2} \left(\frac{r}{r_s} + 1\right)^{3/2}}. \quad (3)$$

Inserting Eq. (3) in the mass profile relation we obtain

$$M_D = 4\pi \int_0^r \frac{\rho_s r'^2}{\left(\frac{r'}{r_s}\right)^{5/2} \left(\frac{r'}{r_s} + 1\right)^{3/2}} dr' = \frac{8\pi\rho_s r_s^3}{\sqrt{1 + \frac{r_s}{r}}}. \quad (4)$$

In a spherically symmetric spacetime, the mass distribution at the center of the DM halo can be used to calculate the tangential velocity of the particle moving within it as follow:

$$v_D^2 = \frac{M_D}{r} = \frac{8\pi\rho_s r_s^3}{r\sqrt{1 + \frac{r_s}{r}}}. \quad (5)$$

A pure DM halo can be described by a spherically symmetric line element:

$$ds^2 = -A(r) dt^2 + \frac{dr^2}{B(r)} + r^2 (d\theta^2 + \sin^2 \theta d\phi^2), \quad (6)$$

where $A(r)$ represents the redshift functions, and $B(r)$ represents the shape functions. It is important to highlight that this BH metric (6) comply with Newtonian approximate, thus $A(r) = B(r)$. The metric function $A(r)$ is related to the tangential velocity through the relation

$$v_D^2 = r \frac{d}{dr} \left(\ln \sqrt{A(r)} \right). \quad (7)$$

Solving for $A(r)$ we obtain

$$A(r) = \exp \left[-32\pi\rho_s r_s^3 \sqrt{\frac{r+r_s}{r_s^2 r}} \right] \approx 1 - 32\pi\rho_s r_s^3 \sqrt{\frac{r+r_s}{r_s^2 r}}, \quad (8)$$

where a leading order term was retained in the equation.

The second step follows Xu's method [45], which has also been used by others [14, 43, 48–51], is to solve Einstein's field equation for a Dehnen-type DM halo distribution and a point mass distribution. When the Dehnen-type DM halo profile completely determines the energy momentum tensor $T_{\mu\nu}$, Einstein's field equation follows.:

$$R_{\mu\nu} - \frac{1}{2}Rg_{\mu\nu} = \kappa^2 T_{\mu\nu}(D) \quad (9)$$

where $\kappa^2 = 8\pi$, $R_{\mu\nu}$ denotes the Ricci tensor, R the Ricci scalar $g_{\mu\nu}$ is the metric tensor. In addition, $T_{\mu\nu}(D)$ denotes the energy-momentum tensor of the Dehnen type DM halo spacetime, which can be written as $T_\mu^\nu = g^{\nu\alpha}T_{\mu\alpha} = \text{diag}[-\rho, p_r, p, p]$. Thus, the Einstein's field equation become

$$\kappa^2 T_t^t(D) = B(r) \left(\frac{1}{r} \frac{B'(r)}{B(r)} + \frac{1}{r^2} \right) - \frac{1}{r^2}, \quad (10)$$

$$\kappa^2 T_r^r(D) = B(r) \left(\frac{1}{r} \frac{A'(r)}{A(r)} + \frac{1}{r^2} \right) - \frac{1}{r^2}, \quad (11)$$

$$\kappa^2 T_\theta^\theta(D) = \frac{1}{2}B(r) \left(\frac{A''(r)A(r) - A'^2(r)}{A^2(r)} + \frac{A'^2(r)}{2A^2(r)} + \frac{1}{2} \left(\frac{A'(r)}{A(r)} + \frac{B'(r)}{B(r)} \right) + \frac{A'(r)B'(r)}{2A(r)B(r)} \right). \quad (12)$$

$$\kappa^2 T_\phi^\phi(D) = \kappa^2 T_\theta^\theta(D) \quad (13)$$

Following [45], for the combined system of the Schwarzschild BH and the DM halo, the spacetime metric can be written as

$$ds^2 = -(A(r) + F_1(r)) dt^2 + \frac{1}{B(r) + F_2(r)} dr^2 + r^2 (d\theta^2 + \sin^2 \theta d\phi^2), \quad (14)$$

where the functions $F_1(r)$ and $F_2(r)$ are determined by BH parameters and DM halo parameters. Therefore, the Einstein field equation can now be written as

$$R_{\mu\nu} - \frac{1}{2}Rg_{\mu\nu} = \kappa^2 [T_{\mu\nu}(D) + T_{\mu\nu}(BH)], \quad (15)$$

where $T_{\mu\nu}(BH)$ arises from the matter content of the pure BH spacetime. Using the combined spacetime metric (14), then the field equation (15) can be simplified as

$$(B(r) + F_2(r)) \left(\frac{1}{r} \frac{B'(r) + F_2'(r)}{B(r) + F_2(r)} + \frac{1}{r^2} \right) = B(r) \left(\frac{1}{r} \frac{B'(r)}{B(r)} + \frac{1}{r^2} \right), \quad (16)$$

$$(B(r) + F_2(r)) \left(\frac{1}{r} \frac{A'(r) + F_1'(r)}{A(r) + F_1(r)} + \frac{1}{r^2} \right) = B(r) \left(\frac{1}{r} \frac{A'(r)}{A(r)} + \frac{1}{r^2} \right), \quad (17)$$

Taking Schwarzschild BH as the boundary condition, then, one obtains the solutions to the above differential equations as

$$F_2(r) = \frac{-2M}{r}. \quad (18)$$

$$F_1(r) = \exp \left[\int \frac{B(r)}{B(r) - \frac{2M}{r}} \left(\frac{1}{r} + \frac{A'(r)}{A(r)} \right) dr \right] - A(r), \quad (19)$$

Based on the assumption of $A(r) = B(r)$, we find that $F_1(r) = F_2(r) = \frac{-2M}{r}$. Therefore, the Schwarzschild BH in the Dehnen-(1, 4, 5/2) DM halo can be written as

$$ds^2 = -f(r) dt^2 + \frac{dr^2}{f(r)} + r^2 (d\theta^2 + \sin^2 \theta d\phi^2), \quad (20)$$

where

$$f(r) = 1 - \frac{2M}{r} - 32\pi\rho_s r_s^3 \sqrt{\frac{r+r_s}{r_s^2 r}}. \quad (21)$$

Fig. 1 depicts how parameters ρ_s and r_s affect the lapse function $f(r)$ for various values. As both parameter values grow, so does the horizon. This plot clearly shows how core density and core radius of the DM halo play a significant role in BH horizons' existence. The horizons of the Schwarzschild-like BH surrounded by a Dehnen type DM halo can be found using the constraint $f(r) = 0$. Each combination of the DM halo parameters ρ_s and r_s results in a unique horizon which is given by

$$r_h = \frac{2M + 512\pi^2 r_s^5 \rho_s^2 + 32\sqrt{2}\pi r_s^2 \rho_s \sqrt{2M^2 + Mr_s + 128\pi^2 r_s^6 \rho_s^2}}{1 - 1024\pi^2 r_s^4 \rho_s^2}. \quad (22)$$

Fig. 2 shows how the horizon depends on the parameters ρ_s and r_s , indicating that the horizon increases with these parameters.

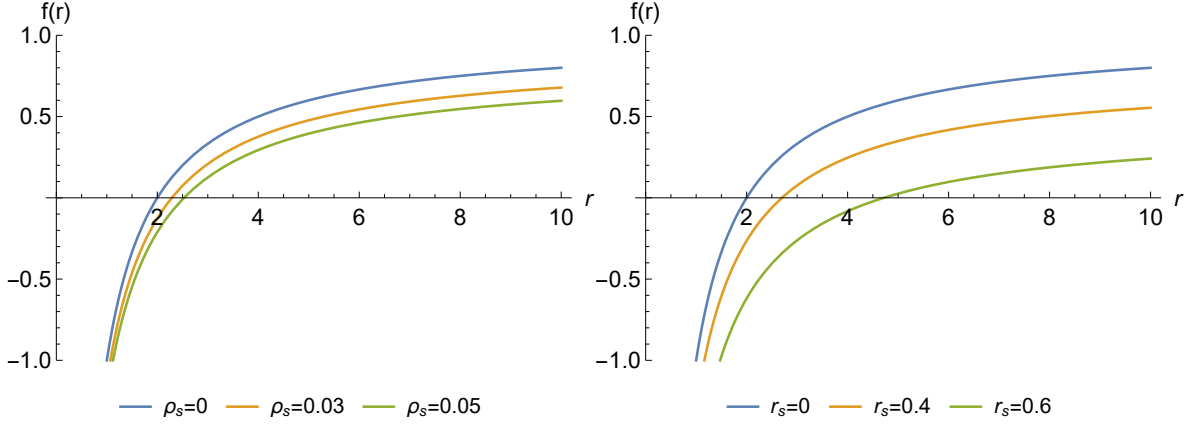


FIG. 1: Lapse function $f(r)$ for varying values of ρ_s by setting $r_s = 0.2$ (left) and for varying values of r_s by setting $\rho_s = 0.015$ (right)

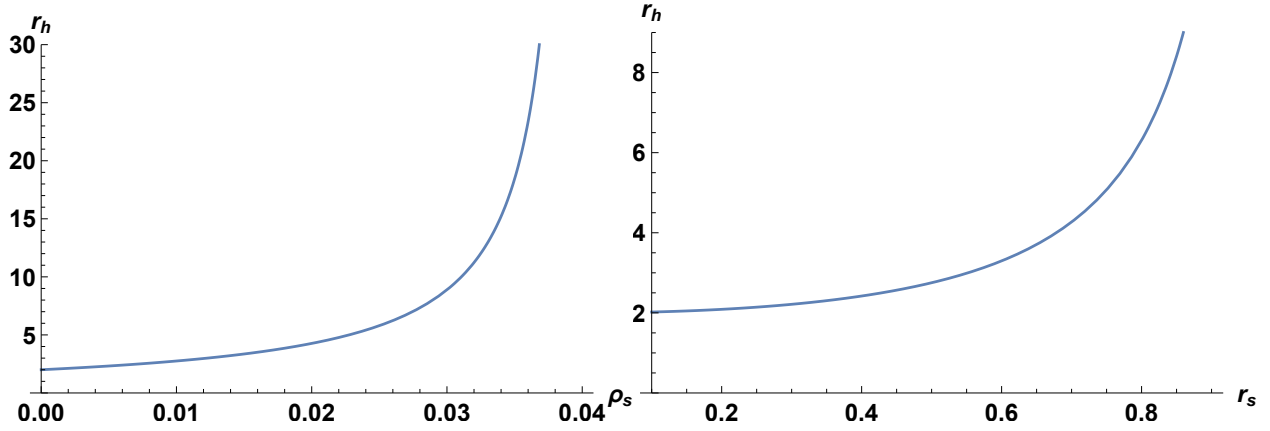


FIG. 2: Variation of horizon r_h for varying values of ρ_s by setting $r_s = 0.5$ (left) and for varying values of r_s by setting $\rho_s = 0.01$ (right)

III. CURVATURE PROPERTIES AND ENERGY CONDITIONS

To examine the singularity structure of this BH (20) at $r = 0$, it becomes crucial to analyse the curvature invariants of the spacetime such as Ricci scalar, R , Ricci square, $R_{\mu\nu}R_{\mu\nu}$, and Kretshmann scalars, $R_{\mu\nu\alpha\beta}R_{\mu\nu\alpha\beta}$.

$$R = \frac{8\pi r_s^2 \rho_s (8r^2 + 12rr_s + 3r_s^2)}{r^4 \left(\frac{r+r_s}{r}\right)^{3/2}}, \quad (23)$$

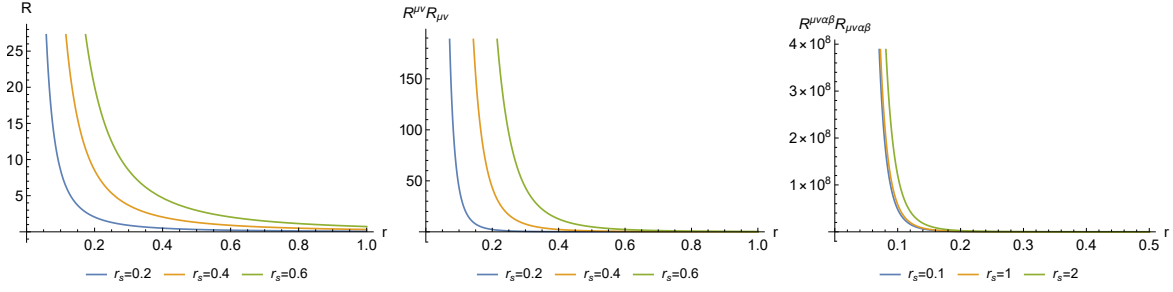


FIG. 3: Variation of Ricci, Ricci squared, and Kretschmann scalar vs r for different values of core radius. Here ($M = 1$ and $\rho_s = 0.01$)

$$R_{\mu\nu}R_{\mu\nu} = \frac{32\pi^2 r_s^4 (64r^4 + 192r^3 r_s + 208r^2 r_s^2 + 96r r_s^3 + 17r_s^4) \rho_s^2}{r^5 (r + r_s)^3}, \quad (24)$$

$$R^{\mu\nu\alpha\beta}R_{\mu\nu\alpha\beta} = \frac{16}{r^8} \left[r^2 \left(M + \frac{8\pi r_s^3 \rho_s}{\sqrt{\frac{r+r_s}{r}}} \right)^2 + r^2 \left(16\pi r r_s^2 \rho_s \sqrt{\frac{r+r_s}{r}} \right)^2 + \left(Mr + \frac{2\pi r_s^3 \rho_s (4r + 3r_s)}{\left(\frac{r+r_s}{r}\right)^{3/2}} \right)^2 \right]. \quad (25)$$

On closer inspection, it appears that the Schwarzschild-like BH solution immersed in Dehnen type DM sets to be singular at the center ($r = 0$) based on the relevant analysis of the invariants (23), (24), and (25). It is therefore possible to obtain the results by inspecting the behavior at the center,

$$\lim_{r \rightarrow 0} R, R_{\mu\nu}R^{\mu\nu}, R_{\mu\nu\alpha\beta}R^{\mu\nu\alpha\beta} \approx \infty. \quad (26)$$

On the other hand, the inspection at large distance shows that

$$\lim_{r \rightarrow \infty} R, R_{\mu\nu}R^{\mu\nu}, R_{\mu\nu\alpha\beta}R^{\mu\nu\alpha\beta} = 0 \quad (27)$$

It states that at large distances, the Ricci scalar, Ricci square, and Kretschmann scalar all have a defined finite term (Fig. 3). Essentially, these invariants show that our BH solution represented by the metric (20) is unique and that there is a physical singularity at $r = 0$.

Our next step is to investigate the energy conditions in Einstein gravity. In view of supplying appropriate physical constraints on the gravitational configuration with matter

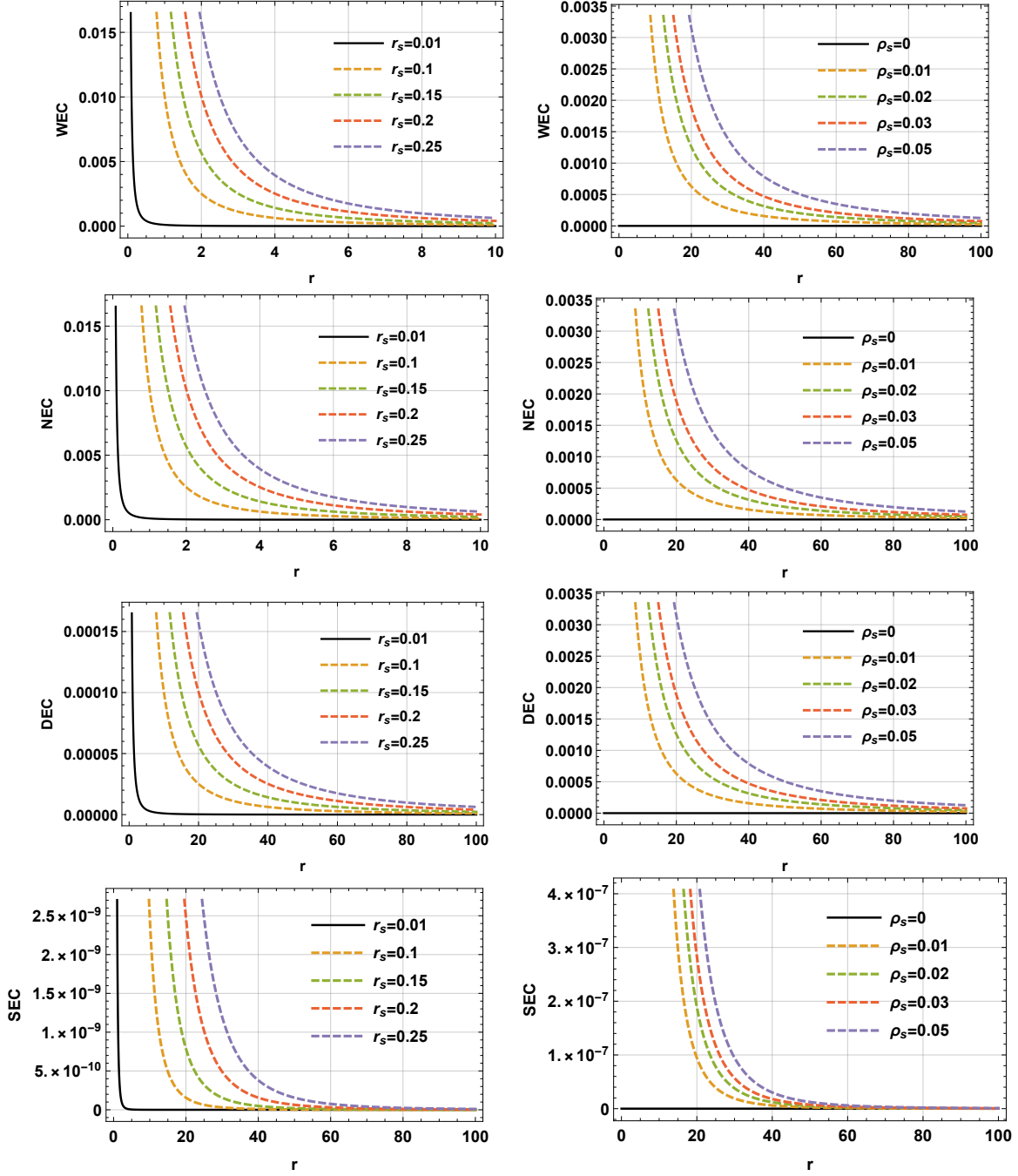


FIG. 4: The variation of ρ (weak energy condition), $\rho + \sum_i P_i$ (strong energy condition), $\rho + P_{\theta,\phi}$ (null energy condition), and $\rho - |P_{\theta,\phi}|$ (dominant energy condition) versus r for multiple values of the parameter r_s with $\rho_s = 0.01$ (left panel) and for multiple value of ρ_s with $r_s = 0.5$ (right panel).

field contribution, we probe the constraints of energy conditions within the resulting BH spacetime [52–55].

The stress-energy tensor elements $T_{\mu\nu}$ ruled by the Einstein equations (15) for the Dehnen-type DM halo BHs consist of the following:

$$\rho = -P_r = \frac{16\pi r_s (r_s + 2r) \rho_s}{r^3 \sqrt{\frac{r_s+r}{rr_s^2}}}, \quad (28)$$

$$P_\theta = P_\phi = \frac{4\pi r_s \rho_s}{r^4 \left(\frac{r_s+r}{rr_s^2}\right)^{3/2}}. \quad (29)$$

By tracking these components, we can proceed to inspect the energy condition constraints to deliver the particular feature in query of the BH solution.

- The weak energy condition (WEC) holds that $T_{\mu\nu} t^\mu t^\nu \geq 0$ anywhere, regardless of the time vector t^μ , which is roughly equated to [56]

$$\rho \geq 0, \quad \rho + P_i \geq 0 \quad (i = r, \theta, \phi) \quad (30)$$

with $\rho + P_r = 0$, so

$$\rho + P_\theta = \frac{4\pi (8r^2 + 12rr_s + 5r_s^2) \rho_s}{r^4 r_s \left(\frac{r_s+r}{rr_s^2}\right)^{3/2}}. \quad (31)$$

The WEC is satisfied if the requirements set out here are fulfilled

$$\frac{16\pi r_s (r_s + 2r) \rho_s}{r^3 \sqrt{\frac{r_s+r}{rr_s^2}}} \geq 0, \quad (32)$$

which demonstrates the perfect satisfaction of the WEC.

- The null energy condition (NEC) implies that $T_{\mu\nu} t^\mu t^\nu \geq 0$ within global space-time for all null vectors t^μ . The NEC demands $\rho + P_r \geq 0$ which is precisely zero, and $\rho + P_\theta = \rho + P_\phi \geq 0$, which is satisfied for the equation (31) whenever the condition is satisfied that

$$\frac{4\pi (8r^2 + 12rr_s + 5r_s^2) \rho_s}{r^4 r_s \left(\frac{r_s+r}{rr_s^2}\right)^{3/2}} \geq 0, \quad (33)$$

predicting full satisfaction of the NEC constraint.

- The dominant energy condition (DEC) states that, in tandem with WEC, whatever the future-directed causal vector field (either temporal or zero) \mathbf{Y} , $-T_{\nu}^{\mu}\mathbf{Y}^{\nu}$ has to be a future-directed causal vector. In other words, mass-energy can apparently always be found to be moving faster than light. On the other hand, DEC requires that $\rho - |P_{\theta,\phi}| \geq 0$ provides the inequality

$$\frac{4\pi(8r^2 + 12rr_s + 3r_s^2)\rho_s}{r^4 r_s \left(\frac{r_s+r}{rr_s^2}\right)^{3/2}} \geq 0, \quad (34)$$

which ensures complete fulfillment of this energy condition.

- The strong energy condition (SEC) asserts that $T_{\mu\nu}t^{\mu}t^{\nu} \geq 1/2 T_{\mu\nu}t^{\nu}t_{\nu}$ overall, just for every time vector t^{μ} which means that [56]

$$\rho + \sum_i P_i = \frac{8\pi r_s \rho_s}{r^4 \left(\frac{r_s+r}{rr_s^2}\right)^{3/2}} \geq 0, \quad (35)$$

so that, the SEC is also satisfied.

The analytical examination of the energy conditions gives intriguing results, allowing us to presume that all the energy conditions are satisfied. The graphical aspect, meanwhile, proves this characteristic for the BHs of the Dehnen-type DM halo. To highlight this behaviour, Fig. 4 offers a suitable graphical analysis that presents the variation of WEC, NEC, DEC, and SEC against the radial spacetime r .

IV. TIMELIKE GEODESICS

Hereafter, we consider timelike geodesics of massive particles with the rest mass m around the Schwarzschild BH surrounded by the Dehnen-(1, 4, 5/2) type DM halo. To this end we first write the Hamiltonian for the given system as follows [57]:

$$H \equiv \frac{1}{2} g^{\alpha\beta} \frac{\partial \mathcal{S}}{\partial x^{\alpha}} \frac{\partial \mathcal{S}}{\partial x^{\beta}}, \quad (36)$$

where S and x^{α} represents the action and the four-vector coordinate, respectively. We then turn to the Hamiltonian of the given system, which is defined by $H = k/2$ with $k/m^2 = -1$. The action S then reads as

$$\mathcal{S} = -\frac{1}{2}k\lambda - Et + L\varphi + \mathcal{S}_r(r) + \mathcal{S}_{\theta}(\theta), \quad (37)$$

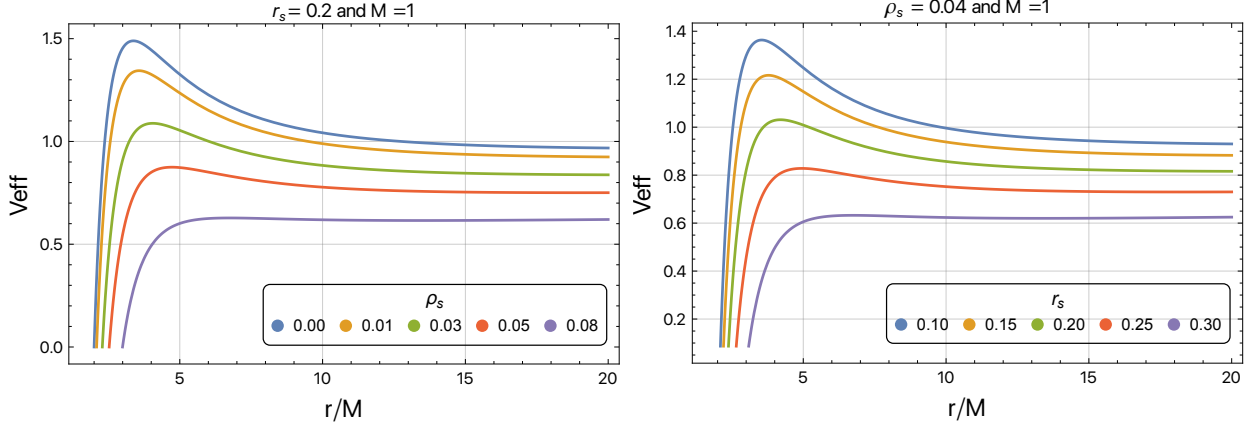


FIG. 5: The effective potential for the timelike motion of particles orbiting around the Schwarzschild BH surrounded by the Dehnen-type DM halo. Left panel: V_{eff} is plotted for different values of the DM density profile parameter ρ_s while keeping r_m fixed. Right panel: V_{eff} is plotted for different values of the halo core radius parameter r_s while keeping ρ_s fixed.

where S_r and S_θ are interpreted as the functions of r and θ , respectively. Eq. (37) allows one to rewrite the Hamilton-Jacobi equation as [31, 32]

$$-\frac{E^2}{f(r)} + f(r) \left(\frac{\partial \mathcal{S}_r}{\partial r} \right)^2 + \frac{1}{r^2} \left(\frac{\partial \mathcal{S}_\theta}{\partial \theta} \right)^2 + \frac{L^2}{r^2 \sin^2 \theta} - k = 0. \quad (38)$$

In the separated form of the Hamilton-Jacobi equation, the four quantities, such as specific energy E , angular momentum L , and k [57], occur as the conserved quantities of the motion, while the fourth one can be ignored when the latitudinal motion takes place at the equatorial plane, $\theta = \pi/2$. Additionally, separable functions S_r and S_θ in the Hamiltonian equation can be defined by

$$S_r = \int \sqrt{E^2 - f(r) \left(-k + \frac{K}{r^2} \right)} \frac{dr}{f(r)}, \quad (39)$$

$$S_\theta = \int \sqrt{K - \frac{L^2}{\sin^2 \theta}} d\theta, \quad (40)$$

where K represents the well-known Carter constant. For making analysis simple, we shall further use

$$\mathcal{E} = \frac{E}{m}, \quad \mathcal{L} = \frac{L}{mM}, \quad \mathcal{K} = \frac{K}{(mM)^2} \quad \text{and} \quad \frac{k}{m^2} = -1. \quad (41)$$

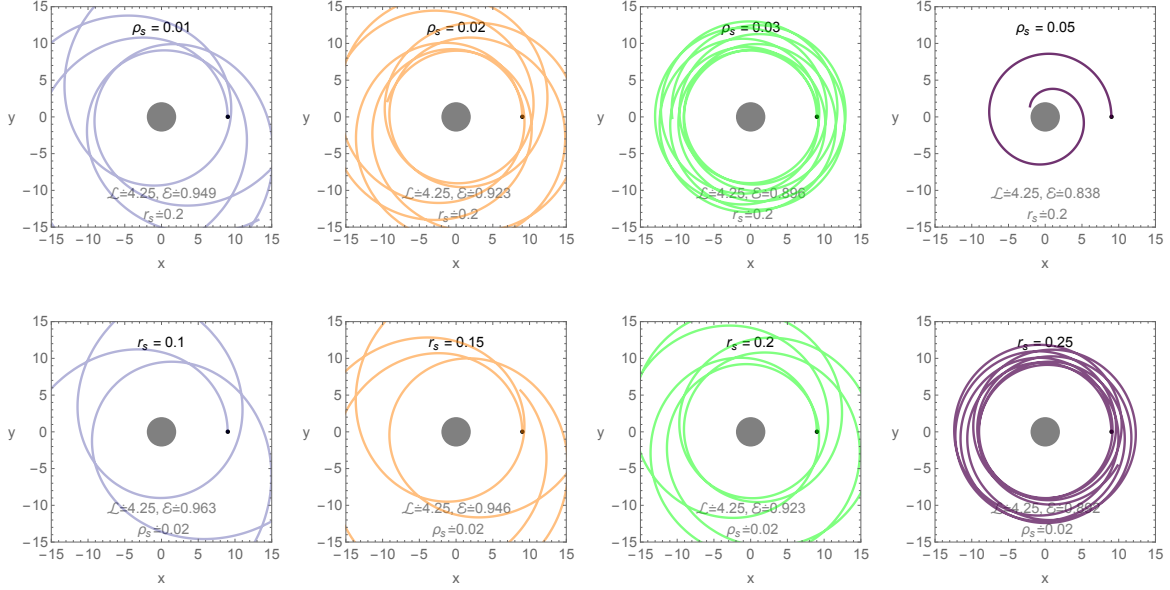


FIG. 6: The geodesics of timelike particles orbiting around the Schwarzschild BH surrounded by the Dehnen-type DM halo for various combinations of the DM halo parameters ρ_s (top row) and r_s (bottom row). Note that the behavior of timelike particle geodesics are observed from the polar view, i.e. $z = 0$.

Following to the Hamiltonian $m dx^\alpha/d\lambda = g^{\alpha\beta}\partial S/\partial x^\beta$ with an affine parameter λ , we define the equations of motion as follows:

$$\dot{t} = \frac{\mathcal{E}}{f(r)}, \quad (42)$$

$$\dot{\phi} = \frac{\mathcal{L}}{r^2 \sin^2 \theta}, \quad (43)$$

$$\dot{r}^2 = \mathcal{E}^2 - f(r) \left(1 + \frac{\mathcal{K}}{r^2}\right) \geq 0, \quad (44)$$

$$\dot{\theta}^2 = \frac{1}{r^4} \left[\mathcal{K} - \frac{\mathcal{L}^2}{\sin^2 \theta} \right] \geq 0. \quad (45)$$

Based on the equations of motion, one can write the timelike radial motion of massive particles orbiting the BH as follows:

$$\dot{r}^2 + V_{\text{eff}}(r) = \mathcal{E}^2, \quad (46)$$

where the radial effective potential $V_{\text{eff}}(r)$ is defined by

$$V_{\text{eff}}(r) = \left(1 - \frac{2M}{r} - 32\pi\rho_s r_s^3 \sqrt{\frac{r+r_s}{r_s^2 r}}\right) \left(1 + \frac{\mathcal{L}^2}{r^2}\right), \quad (47)$$

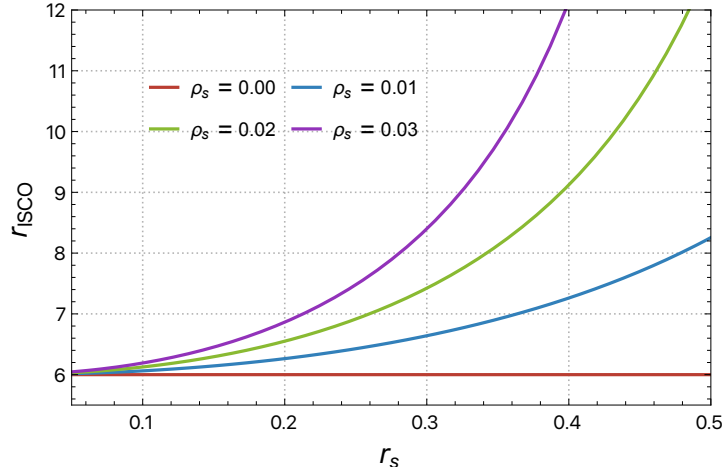


FIG. 7: The ISCO radius of the timelike particles orbiting the Schwarzschild-like BH surrounded by the Dehnen-type DM halo is plotted against the halo core radius parameter r_s for various values of the DM density profile parameter ρ_s .

which determines the particle's radial motion at the equatorial plane, i.e., $\theta = \pi/2$. Now, we turn to analyze $V_{\text{eff}}(r)$ for gaining a deeper understanding of timelike geodesics of particles orbiting the Schwarzschild BH surrounded by the Dehnen-type DM halo.

We shall now analyze the behavior of the effective potential, V_{eff} , for the timelike motion of particles orbiting around the Schwarzschild-like BH surrounded by the Dehnen-type DM halo. In Fig. 5, we show the radial profile of $V_{\text{eff}}(r)$ for the timelike motion. From the figure, one can observe that the left panel reflects the role of the DM profile parameter ρ_s on the effective potential behavior, while the right panel reflects the effect of the halo core radius parameter r_s for various possible scenarios. It is obvious from the plots of the effective potential that the curves slightly shift towards the right to possibly larger r while its maximum shifts downward with an increasing parameter ρ_s , thereby causing the gravitational barrier to weaken. When considering the effects of parameter r_s ranging from 0.1 to 0.3 with equal intervals, corresponding to the curves from up (blue) to down (purple) for the fixed ρ_s , the effective potential changes at a similar rate, resulting in the curves of V_{eff} shifting to the right to possibly larger r , as seen in the right panel of Fig. 5. It is important to note that circular orbits that exist around the BH shift towards the right to larger r from the horizon under the combined effects of both DM halo parameters ρ_s and r_s .

We then turn to the study circular orbits around the BH surrounded by the DM halo. For

the timelike particles to be on the circular orbits, the following required conditions should be satisfied simultaneously

$$V_{\text{eff}}(r) = \mathcal{E}^2 \quad \text{and} \quad V_{\text{eff}}(r)_{,r} = 0, \quad (48)$$

where ", r " refers to a derivative with respect to r . Eq. (48) solves to give the specific angular momentum, \mathcal{L} , of timelike particles orbiting on circular orbits, which is given by

$$\mathcal{L}^2 = \frac{2r^3 f(r) f(r)_{,r} - r^4 f(r)_{,r}^2}{4r^2 f(r)^2 - 4r f(r) f(r)_{,r} + f(r)_{,r}^2}. \quad (49)$$

However, the angular momentum \mathcal{L} allows the effective potential to have extremum points, leading to timelike particles orbiting on circular orbits. It is worth noting, however, that the coincidence of the maximum and minimum of V_{eff} can only occur at the innermost stable circular orbits (ISCOs). For the timelike particles to be on bound orbits, its specific energy \mathcal{E} and angular momentum \mathcal{L} satisfy [58, 59]

$$\mathcal{E}_{\text{ISCO}} \leq \mathcal{E} \leq 1 \quad \text{and} \quad \mathcal{L}_{\text{ISCO}} \leq \mathcal{L}, \quad (50)$$

where $\mathcal{E}_{\text{ISCO}}$ and $\mathcal{L}_{\text{ISCO}}$ respectively refer to the energy and angular momentum of the timelike particle moving on the ISCO around the BH. Note that orbits correspond to captured and escaping ones when particles move on with $\mathcal{E} < \mathcal{E}_{\text{ISCO}}$ and $\mathcal{E} > 1$, respectively. To gain a deeper understanding of these orbits mentioned and to provide some insights into their behavior, we delve into the properties of the DM halo parameters and their effects on the timelike particle geodesics. Therefore, we first qualitatively analyze the timelike particle geodesics observed from the polar view (i.e., $z = 0$) around the BH and demonstrate their behavior in Fig. 6. It is worth noting that for simplicity, we shall focus on the case in which the timelike particles move on orbits restricted to the equatorial plane around the Schwarzschild-like BH surrounded by the Dehnen-type DM halo. As can be seen from Fig. 6, we observe various orbits, such as escaping, bound and captured orbits, depending on the DM halo parameters. This analysis enhances our understanding of the impacts of these parameters in the vicinity of the BH surrounded by the DM halo. From the timelike particle geodesics, as shown in the top row of Fig. 6, one can observe that the orbits are initially escaping ones. However, they turn to be bounded and then eventually captured as ρ_m slightly increases while keeping r_s fixed. Similarly, we can observe similar orbits under the effect of the central halo radius r_s for the fixed ρ_s . That is, the orbits change from

escaping to chaotic behavior and then can slightly be converted into bounded orbits with an increasing parameter r_s ranging from 0.1 to 0.25 with equal intervals, as depicted in the bottom row of Fig. 6.

To determine the ISCO, one needs to solve the following condition

$$V_{eff(r),rr} = 0, \quad (51)$$

providing the minimum orbit particles can move on. We now explore the effects of parameters ρ_s and r_s on the ISCO radius where timelike particles can move around the BH. In Fig. 7, we demonstrate the ISCO radii as a function of the parameter r_s for different combinations of the parameter ρ_s . It is evident from the figure that the ISCO increases and reaches its maximum possible values with an increasing parameter r_s . Similarly, r_{ISCO} changes at a similar rate, causing the ISCO curves to shift upward towards possibly larger values, as shown in Fig. 7. Interestingly, one can infer from the ISCO behavior that it increases to reach larger r under the combined effects of both DM halo parameters ρ_s and r_s .

V. CONCLUSION

From the viewpoint of BH theory, the composition of DM and BH may be an intriguing physical system. In this study, we derive a Schwarzschild-like BH metric in a DM halo with the Dehnen-type density distribution $(1, 4, 5/2)$ and analyze its properties. We first began to examine the singularity structure of this BH at $r = 0$ by analyzing the spacetime curvature invariants. We found that this BH solution represented by the line elements in Eq. (20) is unique and that at $r = 0$, there is a physical singularity. Next, we investigated the energy conditions, focusing on analyzing their behaviors in Einstein gravity. We showed that the analytical evaluation of the energy conditions yields intriguing results, leading us to believe that all of the energy conditions are well met. Meanwhile, the pictorial aspect (Fig. 4) confirms this feature for the BHs in the DM halo with a Dehnen-type density profile.

We also studied the timelike geodesics of particles moving around the Schwarzschild-like BH surrounded by the DM halo with the Dehnen-type density distribution. We showed that the effective potential curves slightly shift towards the right to possibly larger r while its maximum shifts downward as the parameters ρ_s and r_s increase. This behavior results in the weakening of the gravitational barrier, as seen in Fig. 5. We can infer that circular orbits

around the BH can be extended to larger r as a consequence of the combined effects of the DM halo parameters ρ_s and r_s . Additionally, we qualitatively analyzed the timelike particle trajectories observed from the polar view (i.e., $z = 0$) to gain insights into their behavior under the effects of the DM halo parameters. This is a crucial tool for understanding the behavior of timelike geodesics in gravity under different possible cases, facilitating an enhanced understanding of the effects of DM halo parameters ρ_s and r_s on the particle geodesics around the BH. We showed various orbits, including escaping, bound, and captured orbits, depending on the DM halo parameters. It was shown that the orbits are initially escaping and become bounded, eventually being captured as ρ_s slightly increases. Similarly, these orbits change at a similar rate from escaping to chaotic behavior and then become bounded orbits under the effect of the central halo radius r_s for the fixed ρ_s , as depicted in Fig. 6.

Finally, as a consequence of the effects of the DM halo parameters ρ_s and r_s , we examined the behavior of the ISCO radii. We showed that the ISCO changes at a similar rate under the impacts of these DM halo parameters, resulting in r_{ISCO} increasing to reach larger r with the rise in ρ_s and r_s .

Given the importance of the DM halo surrounding supermassive BHs at the center of host galaxies, our approach would be of primary astrophysical significance. It does not exclude the BH solution with a DM halo within a Dehnen-type density distribution $(1, 4, 5/2)$ that could serve as an alternative source of DM halo and play a crucial role in providing insights into the nature of the DM halo.

-
- [1] M. J. Rees, *Annu. Rev. Astron. Astrophys.* **22**, 471 (1984).
 - [2] J. Kormendy and D. Richstone, *Annu. Rev. Astron. Astrophys.* **33**, 581 (1995).
 - [3] G. Bertone and T. M. P. Tait, *Nature* **562**, 51 (2018), [arXiv:1810.01668 \[astro-ph.CO\]](#) .
 - [4] V. C. Rubin and J. Ford, W. Kent, *Astrophys. J.* **159**, 379 (1970).
 - [5] E. Corbelli and P. Salucci, *Mon. Not. Roy. Astron. Soc.* **311**, 441 (2000), [arXiv:astro-ph/9909252 \[astro-ph\]](#) .
 - [6] E. Komatsu and et al. (WMAP Collaboration), *Astrophys. J. Suppl.* **192**, 18 (2011), [arXiv:1001.4538 \[astro-ph.CO\]](#) .

- [7] M. Davis, G. Efstathiou, C. S. Frenk, and S. D. M. White, *Astrophys. J.* **292**, 371 (1985).
- [8] C. Boehm and P. Fayet, *Nucl. Phys. B* **683**, 219 (2004), [arXiv:hep-ph/0305261 \[hep-ph\]](#) .
- [9] G. Bertone, D. Hooper, and J. Silk, *Phys. Rep.* **405**, 279 (2005), [arXiv:hep-ph/0404175 \[hep-ph\]](#) .
- [10] J. L. Feng, M. Kaplinghat, H. Tu, and H.-B. Yu, *J. Cosmol. Astropart. Phys.* **2009**, 004 (2009), [arXiv:0905.3039 \[hep-ph\]](#) .
- [11] M. Schumann, *J. Phys. G Nucl. Part. Phys.* **46**, 103003 (2019), [arXiv:1903.03026 \[astro-ph.CO\]](#) .
- [12] Y. Sofue, *Galaxies* (2020).
- [13] D. Clowe, M. Bradač, A. H. Gonzalez, M. Markevitch, S. W. Randall, C. Jones, and D. Zaritsky, *Astrophys. J. Lett.* **648**, L109 (2006), [arXiv:astro-ph/0608407 \[astro-ph\]](#) .
- [14] K. Jusufi, M. Jamil, and T. Zhu, *Eur. Phys. J. C* **80**, 354 (2020), [arXiv:2005.05299 \[gr-qc\]](#) .
- [15] A. Das, A. Saha, and S. Gangopadhyay, *Classical and Quantum Gravity* **39**, 075005 (2022).
- [16] M. Karamazov, L. Timko, and D. Heyrovský, *Astrophys. J.* **922**, 72 (2021), [arXiv:2103.16965 \[astro-ph.GA\]](#) .
- [17] Qi, Qi, Meng, Yuan, Wang, Xi-Jing, and Kuang, Xiao-Mei, *Eur. Phys. J. C* **83**, 1043 (2023).
- [18] G. Bertone, D. Hooper, and J. Silk, *Phys. Rep.* **405**, 279 (2005), [arXiv:hep-ph/0404175 \[hep-ph\]](#) .
- [19] J. G. de Swart, G. Bertone, and J. van Dongen, *Nature Astron.* **1**, 0059 (2017), [arXiv:1703.00013 \[astro-ph.CO\]](#) .
- [20] R. H. Wechsler and J. L. Tinker, *Annu. Rev. Astron. Astrophys.* **56**, 435 (2018), [arXiv:1804.03097 \[astro-ph.GA\]](#) .
- [21] M. Valluri, D. Merritt, and E. Emsellem, *Astrophys. J.* **602**, 66 (2004), [arXiv:astro-ph/0210379 \[astro-ph\]](#) .
- [22] K. Akiyama and et al. (Event Horizon Telescope Collaboration), *Astrophys. J.* **875**, L1 (2019), [arXiv:1906.11238 \[astro-ph.GA\]](#) .
- [23] K. Akiyama and et al. (Event Horizon Telescope Collaboration), *Astrophys. J.* **875**, L6 (2019), [arXiv:1906.11243 \[astro-ph.GA\]](#) .
- [24] K. Akiyama and et al. (Event Horizon Telescope Collaboration), *Astrophys. J. Lett.* **930**, L12 (2022).
- [25] M. Persic, P. Salucci, and F. Stel, *Mon. Not. R. Astron. Soc.* **281**, 27 (1996), [arXiv:astro-](#)

- ph/9506004 [astro-ph] .
- [26] M.-H. Li and K.-C. Yang, *Phys. Rev. D* **86**, 123015 (2012), arXiv:1204.3178 [astro-ph.CO] .
- [27] S. H. Hendi, A. Nemati, K. Lin, and M. Jamil, *Eur. Phys. J. C* **80**, 296 (2020), arXiv:2001.01591 [gr-qc] .
- [28] M. Rizwan, M. Jamil, and K. Jusufi, *Phys. Rev. D* **99**, 024050 (2019), arXiv:1812.01331 [gr-qc] .
- [29] S. Shaymatov, B. Ahmedov, and M. Jamil, *Eur. Phys. J. C* **81**, 588 (2021).
- [30] J. Rayimbaev, S. Shaymatov, and M. Jamil, *Eur. Phys. J. C* **81**, 699 (2021), arXiv:2107.13436 [gr-qc] .
- [31] S. Shaymatov, D. Malafarina, and B. Ahmedov, *Phys. Dark Universe* **34**, 100891 (2021), arXiv:2004.06811 [gr-qc] .
- [32] S. Shaymatov, P. Sheoran, and S. Siwach, *Phys. Rev. D* **105**, 104059 (2022), arXiv:2110.10610 [gr-qc] .
- [33] V. Cardoso, K. Destounis, F. Duque, R. P. Macedo, and A. Maselli, *Phys. Rev. D* **105**, L061501 (2022), arXiv:2109.00005 [gr-qc] .
- [34] X. Hou, Z. Xu, M. Zhou, and J. Wang, *J. Cosmol. Astropart. Phys.* **2018**, 015 (2018), arXiv:1804.08110 [gr-qc] .
- [35] Z. Shen, A. Wang, Y. Gong, and S. Yin, *Phys. Lett. B* **855**, 138797 (2024), arXiv:2311.12259 [gr-qc] .
- [36] J. F. Navarro, C. S. Frenk, and S. D. M. White, *Astrophys. J.* **462**, 563 (1996), arXiv:astro-ph/9508025 [astro-ph] .
- [37] A. Dutton and A. Macciò, *Mon. Not. Roy. Astron. Soc.* **441**, 3359 (2014).
- [38] D. Merritt, A. W. Graham, B. Moore, J. Diemand, and B. Terzić, *Astron. J.* **132**, 2685 (2006), arXiv:astro-ph/0509417 [astro-ph] .
- [39] A. Burkert, *Astrophys. J. Lett.* **447**, L25 (1995), arXiv:astro-ph/9504041 [astro-ph] .
- [40] W. Dehnen, *Mon. Not. R. Astron. Soc.* **265**, 250 (1993).
- [41] Shukirgaliyev, B., Otebay, A., Sobolenko, M., Ishchenko, M., Borodina, O., Panamarev, T., Myrzakul, S., Kalambay, M., Naurzbayeva, A., Abdikamalov, E., Polyachenko, E., Banerjee, S., Berczik, P., Spurzem, R., and Just, A., *Astron. Astrophys.* **654**, A53 (2021).
- [42] R. C. Pantig and A. Övgün, *J. Cosmol. Astropart. Phys.* **2022**, 056 (2022), arXiv:2202.07404 [astro-ph.GA] .

- [43] M. M. Gohain, P. Phukon, and K. Bhuyan, *Phys. Dark Univ.* **46**, 101683 (2024), [arXiv:2407.02872 \[gr-qc\]](#) .
- [44] T. Matos and D. Nunez, *Rev. Mex. Fis.* **51**, 71 (2005).
- [45] Z. Xu, X. Hou, X. Gong, and J. Wang, *J. Cosmol. Astropart. Phys.* **2018**, 038 (2018), [arXiv:1803.00767 \[gr-qc\]](#) .
- [46] H. Mo, F. C. van den Bosch, and S. White, *Galaxy Formation and Evolution* (Cambridge University Press, Cambridge, 2010).
- [47] J. R. Shakeshaft, ed., *The Formation and Dynamics of Galaxies*, IAU Symposium, Vol. 58 (1974).
- [48] M. Azreg-Aïnou, *Phys. Rev. D* **90**, 064041 (2014), [arXiv:1405.2569 \[gr-qc\]](#) .
- [49] X. Hou, Z. Xu, M. Zhou, and J. Wang, *J. Cosmol. Astropart. Phys.* **2018**, 015 (2018), [arXiv:1804.08110 \[gr-qc\]](#) .
- [50] Z. Xu, J. Wang, and M. Tang, *J. Cosmol. Astropart. Phys.* **2021**, 007 (2021), [arXiv:2104.13158 \[gr-qc\]](#) .
- [51] Y. Yang, D. Liu, A. Övgün, G. Lambiase, and Z.-W. Long, *Eur. Phys. J. C* **84**, 63 (2024), [arXiv:2308.05544 \[gr-qc\]](#) .
- [52] S. W. Hawking and G. F. R. Ellis, *The Large Scale Structure of Space-Time*, Cambridge Monographs on Mathematical Physics (Cambridge University Press, 2023).
- [53] S. G. Ghosh and D. Kothawala, *Gen. Rel. Grav.* **40**, 9 (2008), [arXiv:0801.4342 \[gr-qc\]](#) .
- [54] D. Kothawala and S. G. Ghosh, *Phys. Rev. D* **70**, 104010 (2004), [arXiv:1007.2500 \[gr-qc\]](#) .
- [55] S. G. Ghosh and R. Kumar, *Class. Quant. Grav.* **37**, 245008 (2020), [arXiv:2003.12291 \[gr-qc\]](#) .
- [56] B. Toshmatov, C. Bambi, B. Ahmedov, A. Abdujabbarov, and Z. Stuchlík, *Eur. Phys. J. C* **77**, 542 (2017), [arXiv:1702.06855 \[gr-qc\]](#) .
- [57] C. W. Misner, K. S. Thorne, and J. A. Wheeler, *Gravitation* (W. H. Freeman, San Francisco, 1973).
- [58] N. Dadhich and S. Shaymatov, *Phys. Dark Universe* **35**, 100986 (2022), [arXiv:2104.00427 \[gr-qc\]](#) .
- [59] N. Dadhich and S. Shaymatov, *Int. J. Mod. Phys. D* **31**, 2150120 (2022).